Molecular Therapy
Nucleic Acids
Original Article

Exosomes from Microglia Attenuate Photoreceptor Injury and Neovascularization in an Animal Model of Retinopathy of Prematurity

Wenqin Xu,[1,3] Ying Wu,[2,3] Zhicha Hu,[1] Lijuan Sun,[1] Guorui Dou,[1] Zifeng Zhang,[1] Haiyang Wang,[1] Changmei Guo,[1] and Yusheng Wang[1]

[1]Department of Ophthalmology, Eye Institute of China PLA, Xijing Hospital, Fourth Military Medical University, Xi'an, Shaanxi, China; [2]Department of Thyroid, Breast and Vascular Surgery, Xijing Hospital, Fourth Military Medical University, Xi'an, Shaanxi, China

The role of microglia in the pathophysiology of ischemic retinal diseases has been studied extensively. Exosomes from microglial cells exert protective effects during several nervous system diseases, but their roles in hypoxia-induced retinopathy remain unclear. In our study, exosomes derived from microglial cells were injected into the vitreous body of mice with oxygen-induced retinopathy (OIR). Results showed that exosome-treated OIR mice exhibited smaller avascular areas and fewer neovascular tufts in addition to decreased vascular endothelial growth factor (VEGF) and transforming growth factor β (TGF-β) expression. Moreover, photoreceptor apoptosis was suppressed by exosome injection. Mechanistically, exosomes from microglial cells were incorporated into photoreceptors *in vitro* and inhibited the inositol-requiring enzyme 1α (IRE1α)-X-box binding protein 1 (XBP1) cascade, which contributes to hypoxia-induced photoreceptor apoptosis. Furthermore, the exosomes also downregulated the mRNA and protein levels of VEGF and TGF-β in hypoxia-exposed photoreceptors. A microRNA assay showed that microRNA-24-3p (miR-24-3p) levels were extremely high in exosomes from microglial cells, suggesting that this could be the key molecule that inhibits the hypoxia-induced expression of IRE1α in photoreceptors. These findings delineate a novel exosome-mediated mechanism of microglial cell-photoreceptor crosstalk that facilitates normal angiogenesis and visual function in OIR mice; thus, our results also suggest a potential therapeutic approach for retinopathy of prematurity.

INTRODUCTION

Retinopathy of prematurity (ROP) is known as an ischemic neovascularization disease that mainly affects preterm infants. It has long-term adverse effects on vision development and is considered one of the leading causes of blindness in children worldwide.[1]

In our previous studies, we found that inhibiting microglial activation using minocycline could aggravate visual injury and vasculopathy in mice with oxygen-induced retinopathy (OIR).[2] We also found that microglial density was much higher in BALB/c mice than in C57 mice.[3] Studies also showed that, in a model of OIR, C57 mice exhibited significant vascular destruction and neovascular tuft formation,[4] whereas BALB/c mice, under the same conditions, did not form obvious neovascular tufts, and the central avascular area revascularized very quickly after a return to normoxia.[3] Further differences in retinal microglial density might contribute to the difference in vascular manifestations between these strains.[5]

Microglial cells are traditionally considered innate immune cells, but, recently, the concept that microglial cells are more than just inflammatory cells has become accepted because of the discovery that these cells also participate in normal development of the central nervous system (CNS).[6] Moreover, microglia also takes part in normal vascular development in the retina, which has been demonstrated by several studies.[7–9] However, the role of microglia in vascular development has never been explicitly tested.

Exosomes are small membrane particles, 40∼150 nm in diameter, that form by exocytosis of multivesicular bodies and play diverse biochemical roles in intercellular communication through the transfer of microRNAs (miRNAs), mRNAs, and proteins to recipient cells. Thus, studies of the formation, cargo loading, trafficking, function, and clinical applications of exosomes have increased considerably in recent years.[10]

Recent work has demonstrated that exosomes derived from microglial cells participate in many neurodegenerative diseases.[11,12] Moisseiev et al.[13] have demonstrated that exosomes derived from human mesenchymal stem cells decrease the severity of retinal ischemia in

Received 4 January 2019; accepted 29 April 2019;
https://doi.org/10.1016/j.omtn.2019.04.029.

[3]These authors contributed equally to this work.

Correspondence: Yusheng Wang, Department of Opthalmology, Eye Institute of China PLA, Xijing Hospital, Fourth Military Medical University, Changle West Road, No.15, Xi'an, Shaanxi, China.
E-mail: wangys003@126.com

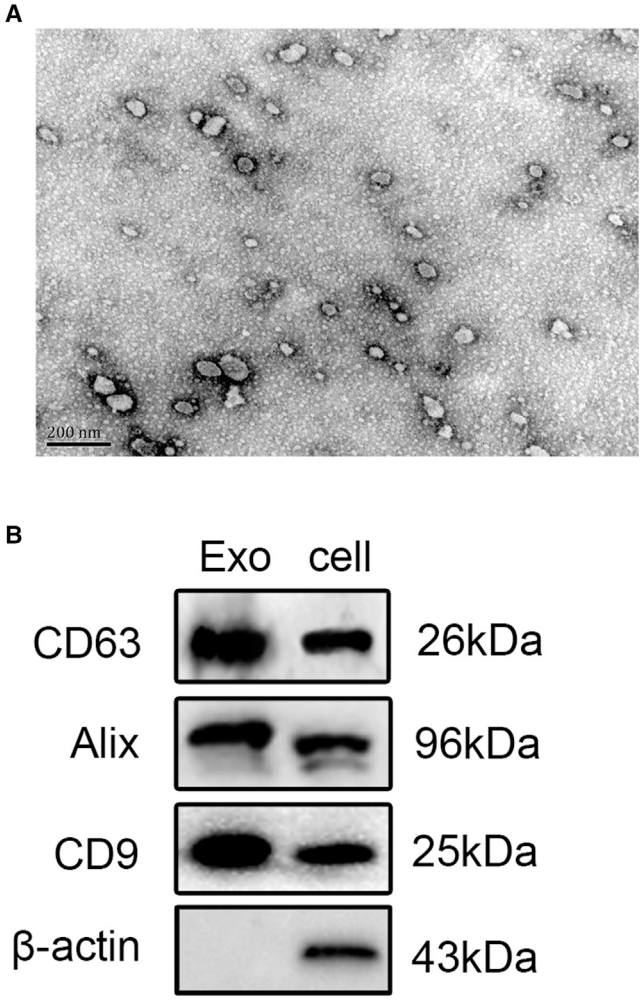

Figure 1. Characterization of Microglia-Derived Exosomes

(A) Transmission electron microscopy (TEM) was used to observe the morphology of microglia-derived exosomes. The diameter of exosomes was approximately 40∼100 nm. Scale bar, 200 nm. (B) Western blot results demonstrating exosome-enriched medium with high expression of the exosome markers Alix, CD9, and CD63 and low levels of β-actin.

OIR mice by protecting retinal cells from death or apoptosis and decreasing retinal neovascular formation.

Here we hypothesize that exosomes derived from microglia could be beneficial for the treatment of photoreceptor injuries and could suppress the secretion of pro-angiogenic factors during ROP, suggesting a better option for ROP treatment. Therefore, the present study primarily investigated whether microglia-derived exosomes (microglia-Exos) could enhance photoreceptor survival and decrease pro-angiogenic factor secretion mediated by hypoxia *in vitro*. More importantly, an OIR model was established, and intravitreal injection of microglia-derived exosomes was performed to detect vasculopathy and changes in visual function.

RESULTS

Characterization of Microglia-Derived Exosomes

Transmission electron microscope (TEM) and western blotting were performed to identify particles purified from microglial cells. The TEM images showed that the extracted particles had a round morphology with a size of approximately 40∼100 nm (Figure 1A). Characteristic biomarkers of exosomes, including Cluster of Differentiation 9 (CD9), CD63, and Alix, were expressed at higher levels in the collected particles than in microglial cell lysates (Figure 1B). These results suggest that particles isolated from microglial cells were highly enriched in exosomes.

Microglia-Derived Exosomes Alleviate Oxygen-Induced Retinal Vaso-obliteration and Neovascularization

To determine whether microglia-derived exosomes could be beneficial for OIR mice, microglia-derived exosomes and an equal volume of PBS were injected into the left and right eye, respectively, on post-natal day 13 (P13). Retinal whole-mount fluorescent staining with isolectin was conducted to visualize the retinal vasculature (Figure 2A). On P16 and P17, the central avascular area in microglia-derived exosome-treated OIR pups was reduced in comparison with that in PBS-treated controls, and some microglia-derived exosome-treated retinas were fully revascularized in the central area, as shown in Figure 2A. More importantly, microglia-derived exosome-treated eyes showed a significant reduction in the area of retinal neovascularization tufts. Further, vascular endothelial growth factor (VEGF) staining of retinal cryosections showed that microglia-derived exosomes significantly decreased the expression of VEGF on P17 (Figure 2B). Retinal VEGF mRNA levels were also measured by real-time qPCR on P16 and P17 after the OIR mice were treated with or without microglia-derived exosomes. As expected, these levels were significantly lower in microglia-derived exosome-treated retinas than in PBS-treated controls (Figure 2C). VEGF protein levels in the retinas of both treatment groups (microglia-derived exosomes and PBS) were also analyzed by western blotting using whole retinal protein extracts and immunostaining. Consistent with the real-time qPCR data, suppression of VEGF expression was apparent in microglia-derived exosome-treated retinas (Figure 2D).

Microglia-Derived Exosomes Alleviate Visual Injury in an OIR Animal Model

We next measured electroretinography (ERG) data on P25 from microglia-derived exosome- and PBS-treated eyes as well as normal eyes. The representative recordings provided a comparison of the b-wave amplitudes of the scotopic and photopic phases, the a- and b-wave maximal amplitudes, and P3 amplitudes of the oscillatory potential (OP) response in PBS- or microglia-derived exosome-treated eyes. It was observed that ERG amplitude was decreased in OIR mice and that microglia-derived exosomes alleviated this injury (Figure 3A).

In the OIR animal model, it has been found that the outer and inner segments of the photoreceptors were disorganized and dysmorphic.[14] Because ERG data demonstrated better visual function in microglia-derived exosome-treated eyes, we expected to see less apoptosis in the

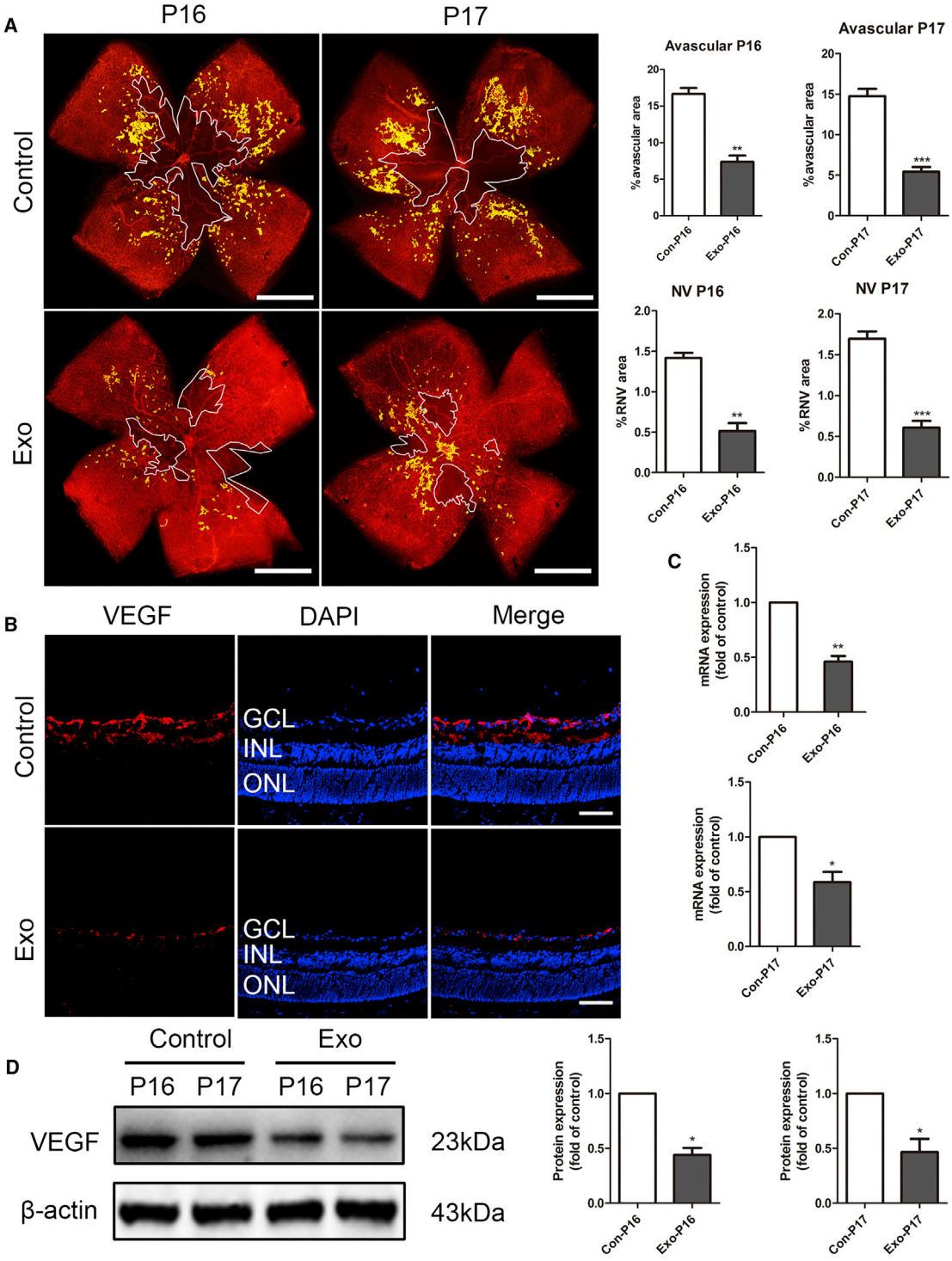

Figure 2. Microglia-Derived Exosomes Inhibit Retinal Neovascular Formation and VEGF mRNA and Protein Expression *In Vivo*

(A) Microglia-derived exosomes promoted re-vascularization of retinal avascular areas and inhibited retinal neovascular areas in oxygen-induced retinopathy (OIR) mice on P16 and P17. Scale bars, 500 μm. (B) Microglia-derived exosomes significantly inhibited VEGF expression in the retinas of OIR mice, which was detected in retinal cryosections. Scale bars, 50 μm. (C and D) Microglia-derived exosomes suppressed VEGF mRNA (C) and protein (D) expression in whole retinas of OIR mice. Microglia-derived exosomes were injected into the vitreous body of OIR mice, and PBS was used as a negative control. All data are expressed as the mean ± S.D., n = 3. *$p < 0.05$, **$p < 0.01$, ***$p < 0.001$ compared with each corresponding control group.

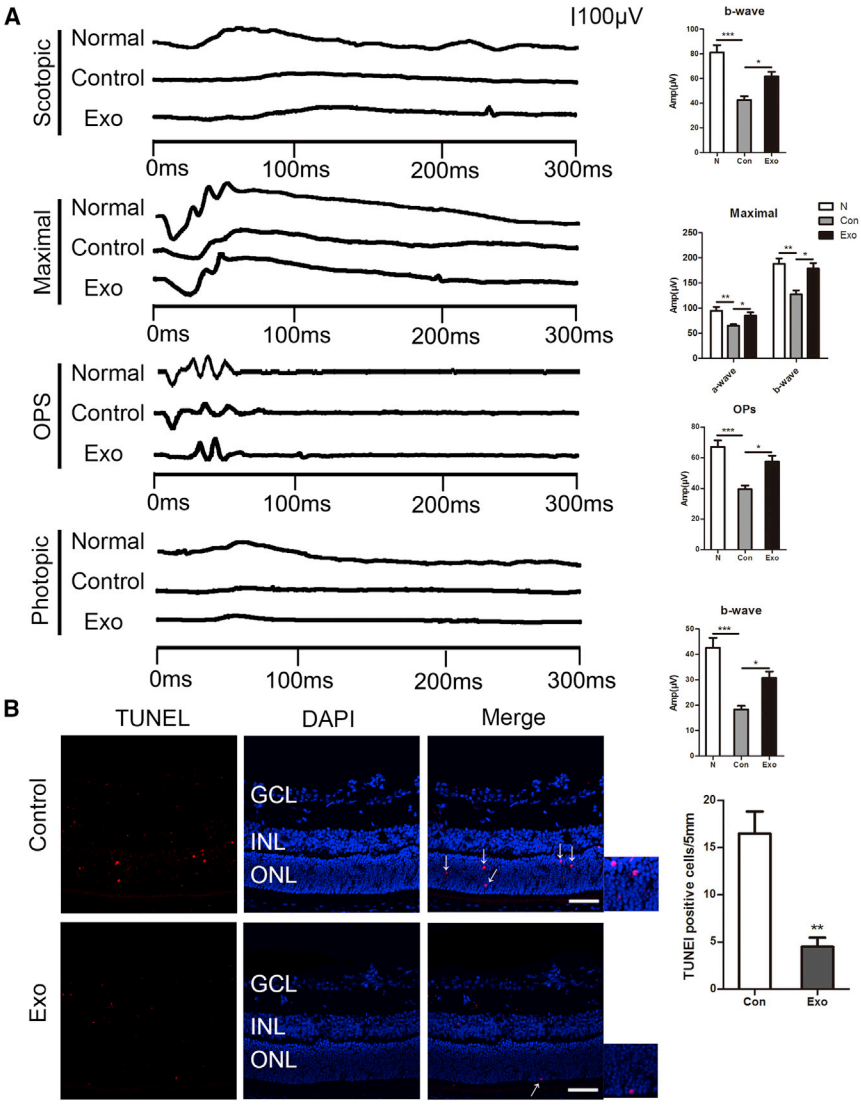

Figure 3. Microglia-Derived Exosomes Improve Visual Function and Decrease Retinal Photoreceptor Apoptosis in OIR Mice

(A) Scotopic electroretinography (ERG) measurements, maximal ERG response, OP measurements, and photopic ERG measurements in the microglia-derived exosomes injection groups, control groups, and normal groups. b-wave amplitude of scotopic ERG and photopic ERG, a- and b-wave amplitude of the maximal ERG response, and the P3 amplitude of OP responses were recorded and compared between microglia-derived exosome injection groups, control groups, and normal groups. (B) Representative images of TUNEL (red) staining in retinal cryosections of microglia-derived exosomes and control groups. Arrows point to the apoptosis nucleus. Quantification of TUNEL-positive cells in the two groups is shown, with the number of TUNEL-positive nuclei (red) in the retina (5 mm in length). Scale bars, 50 μm. All data are expressed as the mean ± S.D., n = 3. *$p < 0.05$, **$p < 0.01$, compared with each corresponding control group.

retinas of these eyes compared with PBS controls. Terminal deoxynucleotidyl transferase (TdT)-mediated DUTP nick end labeling (TUNEL) was used to compare apoptosis in retinas of P17 pups. Figure 3B shows the number of apoptotic nuclei in the retinal outer nuclear layer of PBS-treated and exosome-treated OIR pups. We observed a more than 50% reduction in the number of apoptotic nuclei in microglia-derived exosome-treated retinas compared with PBS controls.

Microglia-Derived Exosomes Alleviate Hypoxia-Induced Photoreceptor Apoptosis by Suppressing Endoplasmic Reticulum (ER) Stress

ER stress is responsible for cell apoptosis, which can be triggered by hypoxia. We first examined whether hypoxia could induce ER stress in 661W cells. As expected, binding immunoglobulin protein (BIP; GRP78), inositol-requiring enzyme 1α (IRE1α), and pancreatic ER kinase (PKR)-like ER kinase (PERK) protein expression levels were induced by hypoxia (1% O_2) (Figure 4A). Western blot results also revealed that hypoxia induced apoptosis in 661W cells in a time-dependent manner. Subsequently, we treated 661W cells with microglia-derived exosomes (at a concentration of 5 μg/mL) and found that this treatment could alleviate hypoxia-induced cell apoptosis (Figure 4B). For this, 661W cells were pre-treated with microglia-derived exosomes for 12 h and then challenged by hypoxia for another 12 h. To illustrate the mechanism by which microglia-derived exosomes decrease apoptosis under conditions of hypoxia, we determined the protein expression of IRE-1α and phosphor-protein kinase-like endoplasmic reticulum kinase (p-PERK) after exosome treatment. We found that IRE1α, but not p-PERK, was significantly decreased. We also measured the protein levels of X-box binding protein 1 (XBP1), CCAAT/enhancer-binding protein homologous protein (CHOP), and phosphorylated c-Jun N-terminal kinase (JNK), which are downstream of IRE1α and associated with apoptosis. Western blotting revealed that microglia-derived exosomes could also decrease IRE1α downstream activation (Figure 4B). Further, knockdown of IRE1α blocked hypoxia-induced apoptosis in 661W cells (Figure 4C). These results indicate that microglia-derived exosomes might alleviate hypoxia-induced apoptosis in 661W cells by inhibiting the IRE1α-XBP-1 pathway.

Microglia-Derived Exosomes Alleviate ER Stress in the Retinas of OIR Mice

IRE1α and its downstream molecules were detected by real-time qPCR or western blotting in P16 and P17 specimens, when

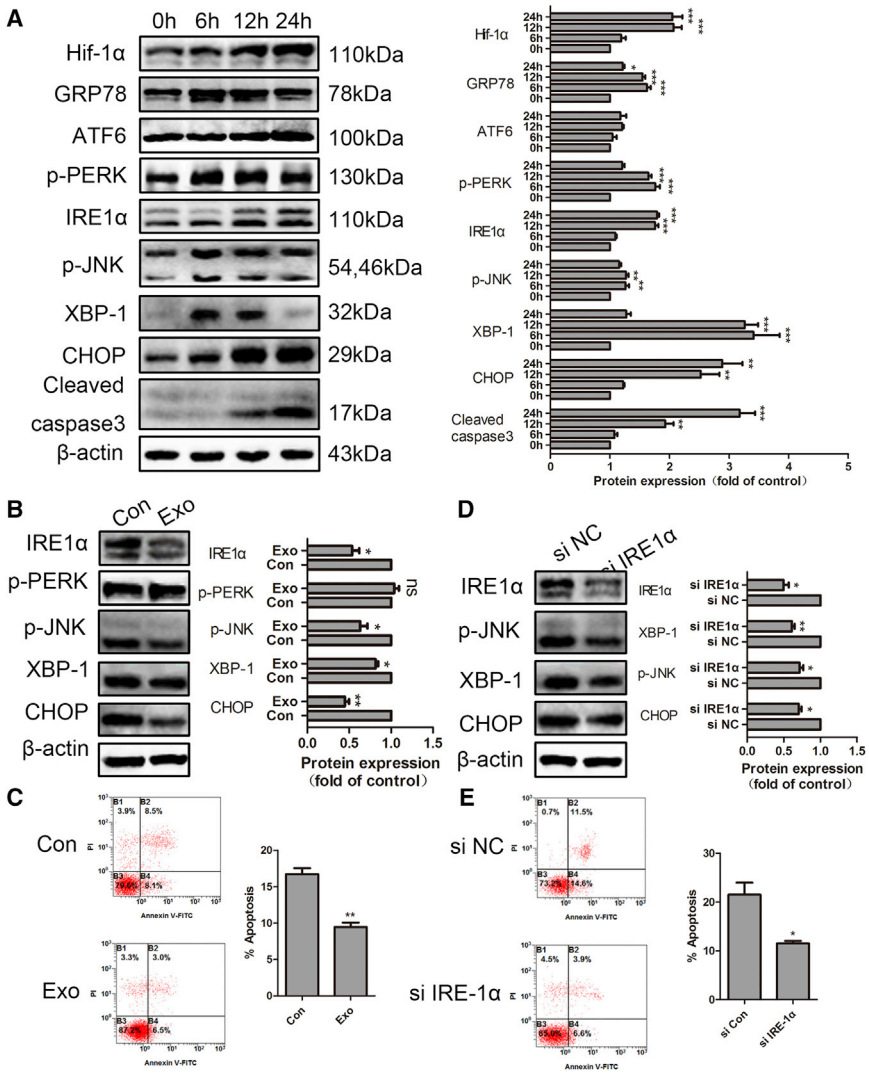

Figure 4. Microglia-Derived Exosomes Alleviate Hypoxia-Induced Photoreceptor Apoptosis by Inhibiting Endoplasmic Reticulum (ER) Stress

(A) Hypoxia was found to increase the expression of Hif-1α, GRP78, p-PERK, IRE1α, p-JNK, XBP-1, CHOP, and Cleaved caspase-3 in 661W cells. (B) Microglia-derived exosomes inhibited the hypoxia-induced increase in IRE1α and downstream molecules but not p-PERK. (C) Microglia-derived exosomes inhibited apoptosis induced by hypoxia in 661W cells. (D and E) Downregulating IRE1α using small interfering RNA (siRNA) decreased p-JNK, XBP-1, and CHOP (D) and apoptosis (E) caused by hypoxia in 661W cells. All data are expressed as the mean ± S.D., n = 3. *p < 0.05, **p < 0.01, ***p < 0.001, compared with each corresponding control group.

neovascular formation is most prominent. The western blot results showed that intravitreal injection of microglia-derived exosomes could decrease the expression of IRE1α, phospho-c-Jun N-terminal kinase (p-JNK), XBP-1, CHOP, and Cleaved caspase-3 in the retinas of OIR mice (Figure 5A). Real-time qPCR was then used to assess CHOP mRNA levels, and the results demonstrated that exosomes could also decrease the expression of this marker in the retinas of OIR mice (Figure 5B).

Detection of miRNA in Microglia-Derived Exosomes

Studies have demonstrated that miRNAs can be delivered between neighboring cells. Here we focused on identification of miRNAs that were transferred from microglia to photoreceptors. We investigated the miRNA expression profiles of microglia-derived exosomes using Illumina HiSeq 2500 high-throughput sequencing (miRNA-seq) and found that miR-24-3p, miR-129-5p, miR-378a-3p, miR-140-3p, miR-151-3p, miR-27b-3p, and miR-21-5p were most highly expressed among the detected miRNAs (Figure 6A). Moreover, real-time qPCR analysis was conducted to determine the levels of these highly expressed miRNAs. Consistent with miRNA-seq, real-time qPCR showed that the levels of miR-24-3p were highest among exosomes derived from microglia.

Microglia-Derived Exosomes Shuttle miR-24-3p into Photoreceptors

To determine whether microglia-derived exosomes could be transferred to 661W cells, microglia-derived exosomes were labeled with PKH67 and then incubated with 661W cells. After 12 h, 661W cells were washed with PBS to remove unbound exosomes, the cytoskeleton was stained with phalloidin, and the nucleus was stained with DAPI. The results showed that PKH67-labeled exosomes were transferred to 661W cells, mainly around the perinuclear region (Figure 6B). To verify the transfer of miR-24-3p to 661W cells, real-time qPCR was performed to estimate miR-24-3p levels in microglia-derived exosome-treated 661W cells. As shown in Figure 6C, miR-24-3p levels in 661W cells were increased significantly after the cells were incubated with microglia-derived exosomes for 12 h. These results indicate that miR-24-3p could be transferred successfully into target cells.

miR-24-3p Mediates the Anti-apoptotic Effects of Microglia-Derived Exosomes on Photoreceptors by Inhibiting IRE1α

We then investigated the effect of miR-24-3p on inhibiting hypoxia-induced photoreceptor apoptosis. First, we found that miR-24-3p mimics had the same effect as microglia-derived exosomes on inhibiting hypoxia-induced apoptosis in 661W cells, whereas the inhibitory effect of microglia-derived exosomes was attenuated by a specific inhibitor targeting miR-24-3p. This indicated that miR-24-3p is responsible for suppressing hypoxia-induced apoptosis in 661W cells. Previous results suggested that the IRE1α-XBP-1 pathway, involved

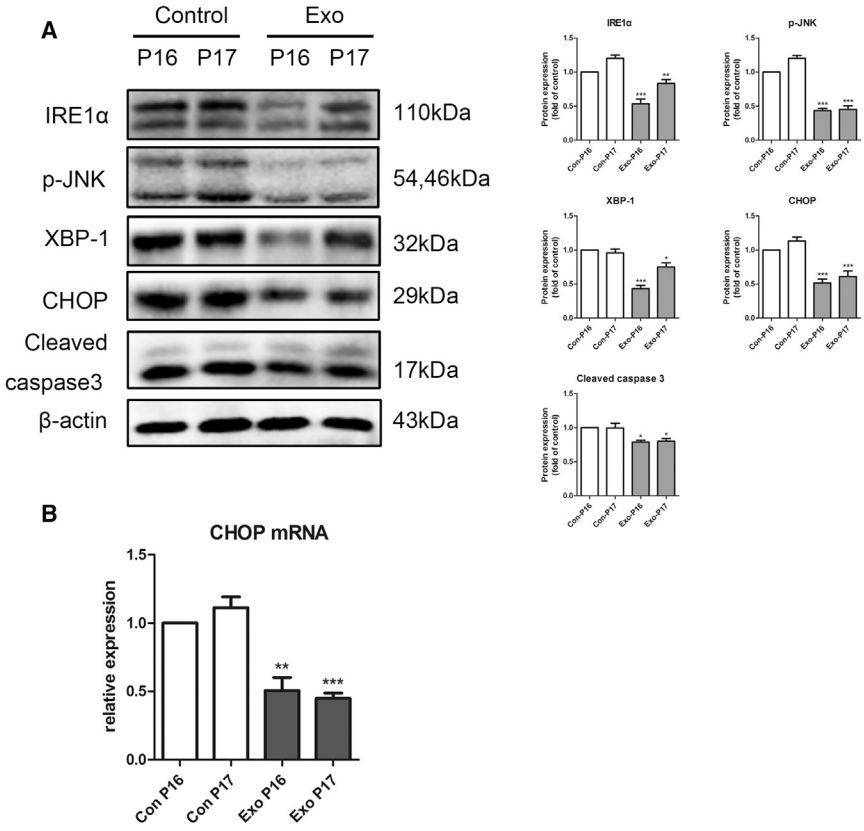

Figure 5. Intravitreal Injection of Microglia-Derived Exosomes Decreases ER Stress in the Retina of OIR Mice

(A) Representative western blot analysis of IRE1α, p-JNK, XBP-1, CHOP, and Cleaved caspase-3 in microglia-derived exosome-treated and control retinas of OIR mice. (B) Relative expression of CHOP mRNA in microglia-derived exosome-treated and control retinas of OIR mice. All data are expressed as the mean ± S.D., n = 3 in each group. *p < 0.05, **p < 0.01, ***p < 0.001, compared with each corresponding control group.

in ER stress, mediates hypoxia-induced 661W cell apoptosis. In addition, it was predicted that ERN1 (IRE1α) is a target of miR-24-3p based on analysis by the TargetScan system (Figure 7A). Western blot analysis confirmed downregulation of IRE1α and downstream molecules in the miR-24-3p mimic group of hypoxic 661W cells, which was similar to that observed in the microglia-derived exosomes group (Figure 7B). Cell apoptosis rates were also decreased in mimic-treated hypoxic 661W cells (Figure 7C). Results also demonstrated that, although microglia-derived exosomes decreased the protein levels of IRE1α in hypoxia-treated 661W cells, a miR-24-3p inhibitor markedly reversed this effect (Figure 7B). Cell apoptosis rates were also higher in inhibitor-treated hypoxic 661W cells than in exosome-treated hypoxic cells (Figure 7C). These results verified that IRE1α is a direct target of miR-24-3p in 661W cells and that microglia-derived exosomes can decrease hypoxia-induced apoptosis by transferring miR-24-3p to target cells.

Microglia-Derived Exosomes Suppress Angiogenic Factor Expression Induced by Hypoxia

To assess the effects of microglia-derived exosomes on the expression of angiogenic factors, hypoxic 661W cells were treated with microglia-derived exosomes or an equal volume of PBS. Real-time qPCR or western blot analysis was then performed to determine VEGF and transforming growth factor β (TGF-β) expression. The results showed that hypoxia significantly promoted the transcription of VEGF and TGF-β, whereas exosome treatment markedly suppressed VEGF and TGF-β mRNA and protein expression as well as phosphorylation of protein kinase B (Akt) and extracellular regulated protein kinase (ERK) (Figure 8A). The conditioned media of normoxic, hypoxic, and microglia-derived exosome-treated hypoxic 661W cells were then used to culture endothelial cells, and tube formation capacity was assessed. The results showed that hypoxic 661W supernatant could promote tube formation *in vitro*, whereas exosome-treated hypoxic supernatant diminished this effect (Figure 8B). These results demonstrated that exosomes might inhibit the expression of angiogenic factors by targeting phosphatidylinositol 3-kinase (PI3K)/Akt and ERK signaling in hypoxic 661W cells and that downregulation of these angiogenic factors can decrease angiogenesis in the retina.

DISCUSSION

Exosomes have been studied for more than 30 years, and recent studies have confirmed that they contain large amounts of small RNAs, especially miRNAs.[15] In our study, we found that exosomes purified from the supernatant of microglial cells alleviated vasculopathy and vision injury in an ROP animal model. We also demonstrated that microglia-derived exosomes could be internalized into photoreceptors *in vitro* and inhibit hypoxia-induced photoreceptor apoptosis via the ER stress pathway and IRE-1α-XBP-1/JNK-CHOP signaling through the transfer of miR-24-3p. We also demonstrated that the exosomes could inhibit the expression of pro-angiogenic factors in photoreceptors *in vitro*, including VEGF and TGF-β, by inhibiting the phosphorylation of Akt and ERK. Our results suggest that microglia might play a beneficial role in ROP. Hypoxia-induced photoreceptor injury is obvious in both ROP infants and OIR animal models.[16,17] It is well known that ROP occurs when the neural retina is still immature. Development of photoreceptors is the last step in maturation of the neural retina, which can be vulnerable to ischemic and hypoxic injury. Clinical ERG data showed that photoreceptor sensitivity is lower in ROP subjects than in age-similar controls in the infancy period and the older age stage.[16–19] Spectral domain OCT (optical coherence tomography) has been used to observe retinal development in

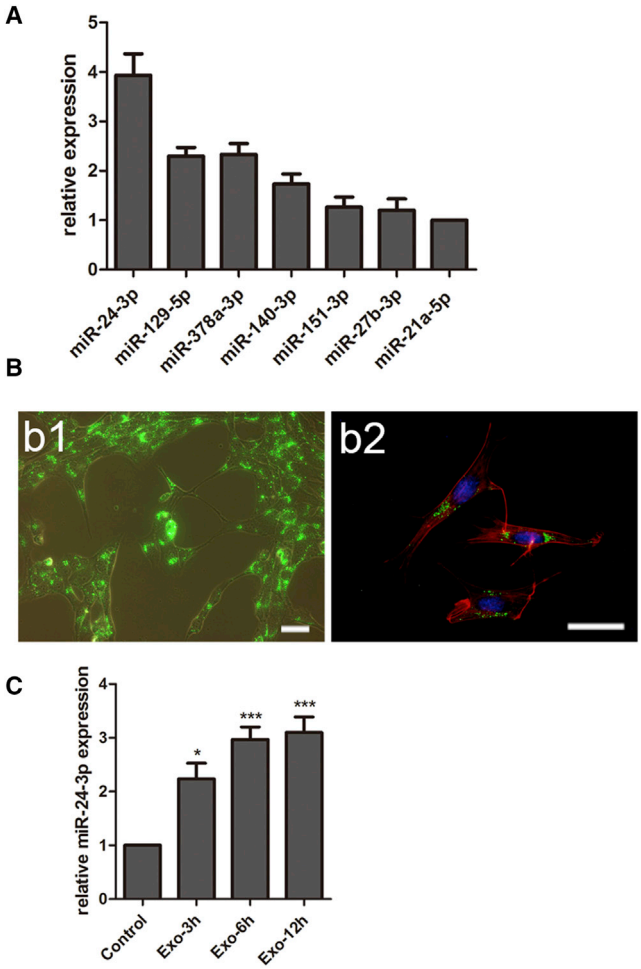

Figure 6. miR-24-3p Is Highly Expressed in Microglia-Derived Exosomes and Can Be Shuttled into Photoreceptors

(A) Ion torrent/microRNA sequencing (MiSeq) found that the highest-expressed miRNAs in microglia-derived exosomes included miR-24-3p, miR-129-5p, miR-378a-3p, miR-140-3p, miR-151-3p, miR-27b-3p, and miR-21a-5p. Real-time qPCR was used to assess the relative expression of these seven miRNAs. (B) Fluorescence microscopy analysis of PKH67-labeled (green) microglia-derived exosome internalization by 661W cells. The cell skeleton was stained with (b2) or without (b1) phalloidin (red), and nuclei were stained with DAPI (blue) (b2). The green-labeled exosomes were visible in the perinuclear region of recipient cells. Scale bars, 20 μm. (C) 661W cells incubated with microglia-derived exosomes exhibited higher levels of miR-24-3p than the control at different time points. All data are expressed as the mean ± S.D., n = 3 per group. *$p < 0.05$, ***$p < 0.001$, compared with the PBS group (control).

infants and analyze retinal structure in ROP patients, and the data showed that the fovea is shallower in ROP subjects than in full term-born individuals. Some researchers have suggested that this might be caused by a failure in centrifugal migration of the post-receptor structure.[20,21] Moreover, in ROP animal models, the b-wave of the ERG was found to be aberrant.[22,23] These data show that photoreceptors are vulnerable and might be impaired in ROP patients and OIR animal models.

In our study, we created a model of hypoxia to assess photoreceptor cells *in vitro* and found that hypoxia led to apoptosis. We also showed that exosomes derived from microglial cells could alleviate hypoxia-induced photoreceptor apoptosis *in vivo* and *in vitro*. Accumulating studies have focused on the mechanism of apoptosis and ER stress.[24–26] Because the ER mediates protein synthesis, folding, and Ca^{2+} maintenance, ER disruption results in apoptosis and death through several mechanisms. In response to ER stress, cells activate the ER stress-specific defense system,[27] and IRE1α acts as the main ER stress transducer;[28,29] however, its role in hypoxia-induced photoreceptor cells was not fully understood. We found that ER stress plays an important role in hypoxia-induced photoreceptor apoptosis. The IRE1α and PERK pathways appear to be activated by hypoxia in photoreceptors, and exosomes derived from microglia have been found to inhibit the increase in IRE1α, but not PERK, which indicates that components of the exosomes might inhibit hypoxia-induced cell apoptosis via the IRE1α pathway but not the PERK pathway. We thus transfected photoreceptors with IRE1α small interfering RNA (siRNA), and the results showed that apoptosis was alleviated, suggesting that microglia-derived exosomes could suppress hypoxia-induced photoreceptor apoptosis mainly by inhibiting IRE1α expression.

miRNAs comprise a class of 20- to 24-nt, small non-coding RNAs that act as inhibitors of target gene expression by inducing mRNA degradation or translational repression. miR-24-3p has been confirmed to prevent apoptosis in several types of cells.[30–32] We found that miR-24-3p was highly expressed in microglia-derived exosomes. After incubation with exosomes, miR-24-3p was highly expressed in photoreceptor cells, indicating that this microRNA could be shuttled to photoreceptor cells and function in these cells. Further, the results showed that upregulating miR-24-3p results in significant inhibition of apoptosis. Based on miRNA target software, we found that IRE1α was a target of miR-24-3p; accordingly, in hypoxia-treated photoreceptor cells, exosomes from microglial cells were found to suppress the expression of IRE1α and downstream molecules associated with ER stress. Addition of miR-24-3p inhibitors to exosome-treated photoreceptors partially reversed the effect of exosomes, indicating that miR-24-3p from microglia-derived exosomes inhibits apoptosis via IRE1α.

Retinal hypoxia is also the main factor leading to upregulation of pro-angiogenetic factors, including VEGF, TGF-β, insulin-like growth factor 1, and erythropoietin, among others, which ultimately leads to the formation of retinal neovascularization.[33,34] Among these, VEGF is considered the most important factor involved in the retinal neovascularization process. Photoreceptors consume abundant amounts of oxygen in the retina, which could aggravate retinal hypoxia and angiogenesis upon hypoxia. Previous results have demonstrated that, in an ROP animal model, VEGF expression was lower in mice with retinal degeneration,[35] which means that photoreceptors could be an important source of pro-angiogenetic factors. We found that hypoxia could increase VEGF and TGF-β mRNA and protein expression in photoreceptors, indicating that photoreceptor cells could be a main source of VEGF and TGF-β in the hypoxic retina.

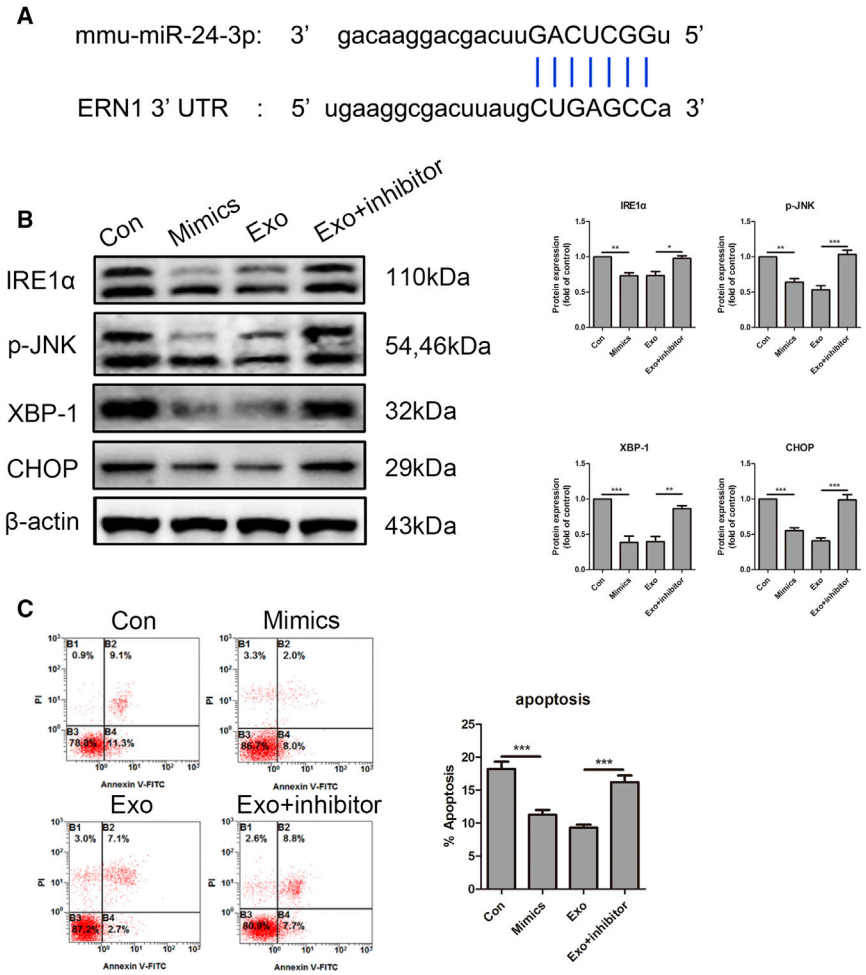

Figure 7. miR-24-3p Exerts Its Functions by Inhibiting IRE1α Expression

(A) The predicted miR-24-3p binding sequence at the 3′ UTR of ERN1 (IRE1α) mRNA. (B) Representative western blot analysis of IRE1α, p-JNK, XBP-1, and CHOP in the miR-24-3p mimic or negative control, exosome-treated, and miR-24-3p inhibitor groups in response to hypoxia. (C) Comparison of apoptosis rates among these four groups. All data are expressed as the mean ± S.D., n = 3. *p < 0.05, **p < 0.01, ***p < 0.001, compared with each corresponding control group.

Therefore, to avoid damage, it is important to prevent photoreceptor apoptosis and inhibit increased expression of pro-angiogenic factors under conditions of hypoxia.

In our study, we found that microglia-derived exosomes could inhibit the elevated expression of VEGF induced by hypoxia. *In vivo*, we found that intravitreal injection of exosomes could decrease the expression of VEGF in the retina of OIR mice on P16 and P17, a time when VEGF is highly expressed and neovascular formation is most obvious. *In vitro*, we also found that hypoxia induces an increase in VEGF in photoreceptor cells, whereas exosomes inhibited this effect. We also used conditioned medium from exosome-treated photoreceptor cells to treat endothelial cells and found that this could dampen tube formation compared with medium from PBS-treated photoreceptor cells. We suggest that resident microglial cells might also have this effect. In our previous studies, we demonstrated that microglial density is substantially different between retinas of C57 mice and BALB/c mice or SD rats. Moreover, animals with higher retinal microglial density exhibited fewer neovascular tufts. We performed intravitreal injection of clodronate liposomes to decrease the density of microglial cells and demonstrated severe retinopathy in a BALB/c OIR model.[3]

This suggests that microglial cells might have an advantageous role in ROP progression and that this effect might occur through exosomes.

It is well known that, in ROP patients, hypoxia induces retinal neovascularization, which is mainly due to upregulation of pro-angiogenic factors, including VEGF. Injection of anti-VEGF antibodies has been shown to be effective for ROP in recent years. Several clinical trials have demonstrated that these, like ranibizumab, can reverse pathologic angiogenic changes, slow down the progression of severe ROP, and induce the development of physiologic retinal vasculature.[36–38]

Studies have also demonstrated possible adverse effects of anti-VEGF therapy in ROP, including suppression of organ development and long-term systemic safety.[39,40] However, it is obvious that regulating VEGF is beneficial for ROP treatment. Exosomes represent a newly emerging mode of communication between cells and have provided new insights into the pathophysiology of several diseases. In recent years, exosomes derived from cells have been considered diagnostic and therapeutic modalities for numerous diseases.[41] In our study, we found that microglia-derived exosomes could have a protective effect against ischemic retinal disease. Our study has some shortcomings. Because it was a mimic of what happens *in vivo*, our findings showed that microglial exosomes could enter photoreceptor cells and play their role. However, we cannot make sure what happened *in vivo*. Therefore, we hope that some studies can check the role of these exosomes in cells in the inner retina or hyaloid, such as endothelial cells. We will design some experiments regarding this in the future.

Primary human microglial cells are not easily characterized and isolated, which is why we did not use these cells in our study. However, some methods are currently used to isolate and culture microglial cells with altered characteristics.[42] Recently, Muffat et al.[43] developed an efficient method to generate microglia-like cells from human embryonic stem cells and induced pluripotent stem cells from control and diseased subjects. Therefore, we hope that autogenous cell-derived exosomes might become a novel treatment option for retinopathy.

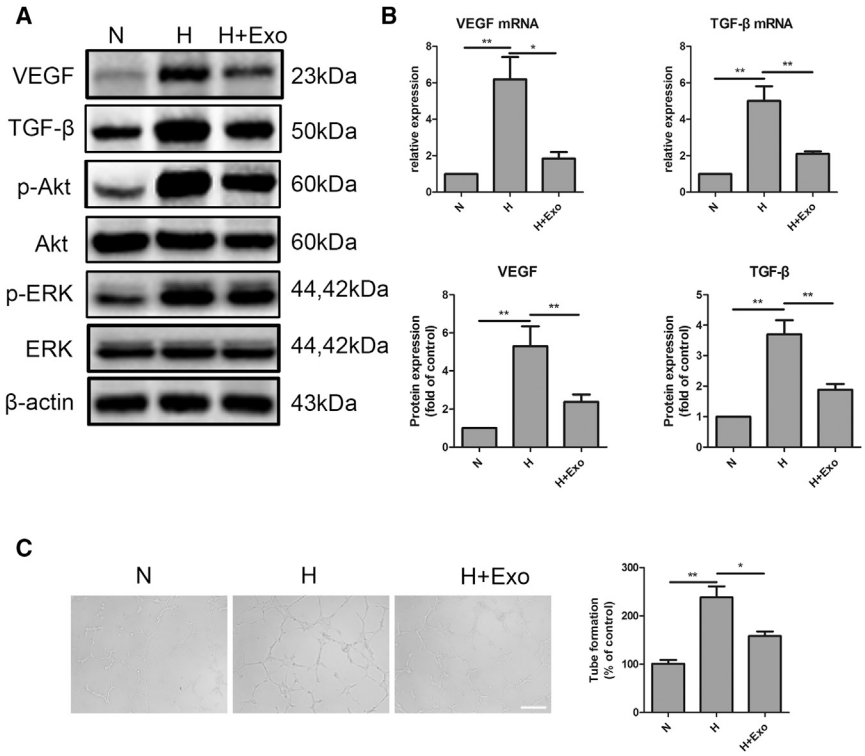

Figure 8. miR-24-3p Inhibits the Expression of Pro-angiogenic Factors by Inhibiting Akt and ERK Activation

(A) Representative western blot analysis of VEGF, TGF-β, p-Akt/Akt, and p-ERK/ERK in normoxia-, hypoxia-, and exosome-administered hypoxia-treated 661W cells. (B) Relative expression of VEGF and TGF-β mRNA and protein in exosome-treated and control 661W cells. (C) Tube formation in endothelial cells exposed to different 661W cell supernatants. Scale bar, 100 μm. All data are expressed as the mean ± S.D., n = 3. *$p < 0.05$, **$p < 0.01$.

MATERIALS AND METHODS

Animals

Mature (8-week-old) C57BL/6J male and female mice were purchased from the animal research center at the Fourth Military Medical University. The protocols we used complied with the NIH Guide for the Care and Use of Laboratory Animals (NIH publication 8023, revised 1978) and the Institutional Animal Ethics Committee of the Fourth Military Medical University.

BV2 Microglial Culture and Microglial Exosome Isolation

BV2 microglial cells were donated by the Institute of Neurosciences at the Fourth Military Medical University. Cells were routinely cultured in DMEM (HyClone, USA) containing 10% fetal bovine serum (FBS; HyClone) at 37°C. For the isolation of exosomes, microglia were cultured in FBS-free DMEM culture for 48 h, and the supernatant of the cell culture medium was collected and centrifuged at 300 × *g* for approximately 10 min to remove free cells. Then the supernatant was transferred into a sterile centrifuge tube. The tubes were centrifuged at 2,000 × *g* for approximately 10 min and then at 10,000 × *g* for 30 min to remove cell debris and cell particles. Then a 0.22-μm filter (Millipore, Sigma) was used to filter the supernatant to remove particles. Ultracentrifugation was used to isolate exosomes at 100,000 × *g* for 70 min. We collected the pelleted exosomes, washed them with PBS, centrifuged them again at 100,000 × *g* for 70 min, and re-suspended the pellet in 100 μL of PBS. All procedures were conducted at 4°C. Exosomes were stored at −80°C for less than 1 week or used immediately for downstream experiments. The bicinchoninic acid method (Beyotime Biotechnology) was used to determine protein concentrations.

Microglial Exosome Identification

For exosome identification, TEM (HT7700; Hitachi, Tokyo, Japan) was used to observe the morphology of particles in the pellets. This method has been described previously.[44] In addition, biomarkers of exosomes, including CD9, CD63, and Alix, were detected by western blot analysis (as described subsequently).

Mouse Model of OIR

The pups, together with their mothers, were placed in a high-oxygen chamber on P7 for 5 days, and the oxygen volume fraction was 75% ± 2%. On P12, all animals were returned to room air (normoxic conditions). The mice were treated with standard water and diet.

Intravitreal Injection of Microglia Exosomes

OIR mice on P13 were anesthetized, and a 2.5-μL 34G Hamilton syringe (Hamilton, Reno, NV, USA) was used to make intravitreal injections; specifically, 1 μL of microglial exosome solution (1 mg/mL) was injected into the vitreous cavity of the left eye, and 1 μL of PBS was injected into the right eye as a control.

Retinal Flatmounts

On P17, mice were anesthetized, and the eyeballs were enucleated and fixed in 4% paraformaldehyde (PFA) for 2∼4 h. Retinas were dissected and placed in 4% PFA overnight and incubated with 1% Triton X-100 and 1% BSA at 4°C overnight. Retinas were then cut into petals and stained with griffonia simplicifolia lectin-isolectin B4 (GSL-IB4) isolectin (1:100, Vector Laboratories, USA) at 4°C for 12 h in the dark. Then we transferred the whole flatmounts to glass slides and observed and captured images using a microscope.

Retinal Cryosections and Immunofluorescence Staining

The enucleated eyes without the cornea, lens, and vitreous were embedded in Tissue-Tek optimal cutting temperature compound (Sakura Finetek, Torrance, USA), and 8-μm serial sections were then produced (CM1800; Leica Instruments, Heidelberg, Germany). The slides were incubated with an anti-VEGF antibody (1:200,

Abcam, UK) in a humidified chamber overnight at 4°C. Then the slides were incubated with secondary antibodies for 3 h at room temperature in the dark, and Alexa Fluor 488-conjugated goat anti-rabbit immunoglobulin G (IgG; Invitrogen) was used. Finally, the slides were labeled with DAPI (Invitrogen) and observed under a FluoView 1000 microscope (Olympus, Japan).

Real-time qPCR Analysis

Total RNA from 661W cells and retinal tissues was extracted using Trizol reagent (Invitrogen, USA) following the manufacturer's protocol. A cDNA synthesis kit (TAKARA, Japan) was used to synthesize cDNA from mRNA. Amplification was then performed using a kit (SYBR Premix EX Taq, TARKARA) and the ABI PRISM 7500 real-time PCR system. β-Actin served as a reference control. The primers used for real-time qPCR were as follows: CHOP-forward: 5′-GGAACCTGAGGAGAGAGTGTTC-3′, CHOP-reverse: 5′-AAGGTGAAAGGCAGGGACTC-3′; VEGF-forward: 5′-TATTCAGCGGACTCACCAGC-3′, VEGF-reverse: 5′-AACCAACCTCCTCAAACCGT-3′; TGF-β-forward: 5′- GACCGCAACAACGCCATCTA-3′, TGF-β-reverse: 5′- GGCGTATCAGTGGGGGTCAG-3′; β-actin-forward: 5′-CATCCGTAAAGACCTCTATGCCAAC-3′, β-actin-reverse: 5′-ATGGAGCCACCGATCCACA-3′.

Quantification of miR-24-3p miR-129-5p, miR-378a-3p, miR-140-3p, miR-151-3p miR-24-3, and miR-21-5p were performed with a stem-loop real-time PCR miRNA kit (Ribobio, Guangzhou, China). miRNA primer was also obtained from Ribobio (Guangzhou, China). Fold induction was calculated using the Ct method: ΔΔCt = (CtTarget miRNA−CtU6) − (CtmiR-21-5p−CtU6), and the final data were derived from 2−ΔΔCt.

The primers used for real-time qPCR were as follows: miR-24-3p-forward: 5′-GCCGAGTGGCTCAGTTCAG-3′, miR-24-3p-reverse: 5′-CTCAACTGGTGTCGTGGA-3′; miR-129-5p-forward: 5′- GCCGAGCTTTTTGCGGTCT-3′, miR-129-5p-reverse: 5′-CTCAACTGGTGTCGTGGA-3′; miR-378a-3p-forward: 5′-GCCGAGACTGGACTTGGAG-3′, miR-378a-3p-reverse: 5′-CTCAACTGGTGTCGTGGA-3′; miR-140-3p-forward: 5′-GCCGAGTACCACAGGGTAGA-3′, miR-140-3p-reverse: 5′-CTCAACTGGTGTCGTGGA-3′; miR-151-3p-forward: 5′-GCCGAGCTAGACTGAGGCT-3′, miR-151-3p-reverse: 5′-CTCAACTGGTGTCGTGGA-3′; miR-24-3p-forward: 5′-GCCGAGTGGCTCAGTTCAG-3′, miR-24-3p-reverse: 5′-CTCAACTGGTGTCGTGGA-3′; miR-21-5p-forward: 5′-GCCGAGTAGCTTATCAGACTG-3′, miR-21-5p-reverse: 5′-CTCAACTGGTGTCGTGGA-3′; U6-forward: 5′-CGCTTCGGCAGCACATATAC-3′, U6-reverse: 5′-TTCACGAATTTGCGTGTCAT-3′.

Western Blot Analysis

Cells or retinal tissue were lysed using lysis buffer (Beyotime Biotechnology, China) containing a protease inhibitor. The bicinchoninic acid method (Beyotime Biotechnology) was used to determine protein concentrations. Then 20 μg of protein was added and fractionated on 10% or 12% SDS-PAGE gels, after which the protein was electroblotted onto polyvinylidene fluoride membranes (Millipore, USA). Next, 5% nonfat dry milk in Tris buffered saline with Tween 20 (TBST) buffer was used to block the membranes. Then the membranes were incubated with primary antibodies overnight at 4°C as follows: anti-CD9 (1:500, Abcam), anti-CD63 (1:200, Abcam), anti-Alix (1:1,000, Abcam), anti-Hif1α (1:1,000, Abcam), anti-GRP78 (1:1,000, Proteintech, Wuhan, China), anti-p-PERK (1:200, Santa, USA), anti-CHOP (1:1,000, Proteintech), anti-XBP1 (1:1,000, Proteintech), anti-ATF6 (1:1,000, Proteintech), anti-IRE1α (1:1,000, Abcam), anti-Cleaved caspase-3 (1:1,000, Cell Signaling Technology, USA), anti-p-JNK (1:1,000, Cell Signaling Technology), anti-p-Akt (1:1,000, Cell Signaling Technology), anti-Akt (1:1,000, Cell Signaling Technology), anti-phosphor-extracellular regulated protein kinase (p-ERK; 1:1,000, Cell Signaling Technology), anti-ERK (1:1,000, Cell Signaling Technology), anti-VEGF (1:1,000, Abcam), and anti-TGF-β (1:1,000, Cell Signaling Technology). After incubation with horseradish peroxidase (HRP)-conjugated secondary antibodies (1:5,000, Santa Cruz Biotechnology) for 2 h at room temperature with gentle agitation. Proteins of interest were detected using the enhanced chemiluminescence method (ECL, Thermo Scientific). Western blots were scanned using a ChemiDoc XRS+ system (Bio-Rad) and semi-quantification was performed using ImageJ 1.40 software, analyzing the intensity of the grayscale images. β-Actin was used as a loading control.

ERG Data

ERG was performed on P25 animals because the vasculature in the retina appeared to be normal. After dark adaption overnight, the mice were deeply anesthetized, and the pupils of the tested eye were dilated with tropicamide eye drops (Shenyang Xingqi, China). An active electrode was then inserted into the cornea of the tested eye, the reference electrode was inserted beneath the cheek mucosa around the tested eye, and the ground electrode was inserted into the skin of the tail. Full-field (ganzfeld) stimulation and the RETI port system (Brandenburg, Germany) were used to document ERG data. In our study, scotopic 0.01 cd.s.m−2, 3.0 cd.s.m−2 (maximal), and 3.0 cd.s.m−2 OP electroretinographs as well as photopic 3.0 cd.s.m−2 and 3.0 cd.s.m−2 flicker electroretinographs were recorded.

In Situ Nick End Labeling (TUNEL)

The *In Situ* Cell Death Detection Kit, TMR red (Sigma-Aldrich) was used to detect apoptosis. All processes were conducted according to the manufacturer's protocol. First, slides were fixed with 4% PFA for approximately 1 h, permeabilized in 0.1% citrate buffer (Beyotime Biotechnology, China) containing 0.1% Triton X-100 (Beyotime Biotechnology) for 2 min on ice, and then incubated in the TUNEL reaction mix at 37°C for 1 h in the dark. The slides were then incubated with DAPI (Vector Laboratories, USA) and observed under an Olympus FluoView 1000 microscope.

661W Photoreceptor Culture

661W cells were obtained from the University of Oklahoma, and these have been widely used for ophthalmic research. Cells were separated from retinal tumors in a transgenic mouse line. 661W cells

express some of the same proteins as photoreceptors, including blue and green cone pigments as well as cone arrestin and transducin.[45,46] These cells were cultured in DMEM/high-glucose medium containing 10% FBS at 37°C in an atmosphere of 5% CO_2.

Cell Apoptosis Analysis by Flow Cytometry

Annexin v-fluorescein isothiocyanate (FITC)/propidium iodide (PI) staining was used to detect apoptosis. According to the protocol, 661W cells were harvested after different treatments, and 100 μL of an Annexin v-FITC and PI (Sigma-Aldrich) mixture was added to the cells. Then flow cytometry was used to detect fluorescent cells. The number of apoptotic cells and the ratio of apoptosis in 661W cells were analyzed using BD FACSuite software.

RNAi

miR-24-3p mimics and inhibitors and their respective negative controls were purchased from RIBOBIO (Guangzhou, China). Cell transfection was performed following the instructions from RIBOBIO. Briefly, 661W cells were planted in 6-well culture plates and then transfected with miR-24-3p mimics (50 nM) and inhibitors (150 nM) using Lipofectamine 2000 (Invitrogen). Then microglia-derived exosomes were added to the plates (5 μg/mL). After 24 h of incubation, downstream experiments were conducted.

For IRE1α depletion, cells were transfected with siRNAs targeting mouse IRE1α (GenePharma, Shanghai, China) using Lipofectamine 2000 (Invitrogen, USA) following the manufacturer's instructions. The negative control was a non-silencing scrambled siRNA. Knockdown efficiency was measured by detecting target protein levels using western blotting.

miRNA Library Construction and Sequencing

Total RNA from exosomes was used for miRNA library preparation and sequencing. The preparation and sequencing of exosome miRNA were performed by Ribobio (Guangzhou, China). A total of 50 mL of cellular supernatant was mixed with Ribo exosome isolation reagent, and exosome isolation was performed according to the manufacturer's instructions (Ribobio, China). Exosomal RNA was extracted by HiPure Liquid miRNA Kit/HiPure Serum/Plasma miRNA Kit (Megan, China). The quantity and integrity of the exosomal RNA yield were assessed by using the Qubit 2.0 (Life Technologies, USA) and Agilent 2200 TapeStation (Agilent Technologies, USA) separately. 50 ng exosomal RNA of the sample was used to prepare small RNA libraries by NEBNext Multiplex Small RNA Library Prep Set for Illumina (New England Biolabs, USA) according to manufacturer's instructions. The libraries were sequenced by HiSeq 2500 (Illumina, USA) with single-end 50 bp at Ribobio (Ribobio, China). For data processing, the raw reads were processed by filtering out poly "N," low quality, smaller than 17 nt reads by FASTQC to get clean reads. Mapping reads were obtained by mapping clean reads to the reference genome by BWA. miRDeep2 was used to identify known mature miRNA based on miRBase21 (http://www.miRBase.org) and predict novel miRNA. miRNA expression was calculated by RPM (reads per million) values (RPM = (number of reads mapping to miRNA/number of reads in clean data) × 10^6). The expression levels were normalized by RPM; RPM = (number of reads mapping to miRNA/number of reads in clean data) × 10^6.

Exosome Uptake by Photoreceptors

To determine microglia-derived exosome uptake by photoreceptors, exosomes were labeled with a green fluorescent dye (PKH67; Sigma, USA) according to the manufacturer's instructions and then incubated with 661W cells at 37°C for 6 h. The cells were then washed with PBS three times and fixed in 4% PFA for 15 min. The cytoskeleton was stained with tetramethylrhodamine (TRITC)-phalloidin reagents (Cell Signaling Technology, USA), and nuclei were stained with DAPI (Invitrogen, USA). Fluorescence microscopy was used to detect exosomes in 661W cells. To detect whether miRNAs could be transferred from exosomes to 661W cells, real-time qPCR analysis (described subsequently) was used to measure the expression of miRNA in the recipient cells that were incubated with exosomes for 3–24 h.

Tube Formation Assays

The RF/6A cell line was purchased from the China Center for Type Culture Collection (CCTCC). Tube formation was performed using RF/6A cells in co-culture with conditioned media from normoxic, hypoxic, and exosome-treated hypoxic photoreceptors *in vitro*. First, 96-well plates were pre-coated with 50 μL of Matrigel (Bedford, USA) for 0.5 h in a cell incubator. Then 1.5 × 10^4 RF/6A cells per well were seeded on the Matrigel and cultured with the supernatant of 661W cells for 6 h. The length of the tubes was measured using Image Pro Plus 6.0 software, and fold changes in tube length were calculated.

Statistical Analysis

Comparisons of means between two groups were analyzed by performing an unpaired Student's t test, whereas a one-way ANOVA with Bonferroni's multiple comparisons correction was used for three groups or more. A value of $p < 0.05$ was considered statistically significant.

AUTHOR CONTRIBUTIONS

W.X. and Y.W. conducted the experiments and wrote the manuscript. Z.H. and L.S. analyzed the data. G.D., Z.Z., H.W., and C.G. helped revise the manuscript. Y.W. designed the experiment, wrote the manuscript, made critical revisions, and approved the final version. All authors read and approved the final manuscript.

CONFLICTS OF INTEREST

The authors declare no competing interests.

ACKNOWLEDGMENTS

The study was supported by National Natural Science Foundation of China grants 81570856, 81770936, 81470655, 81670863, and 81300770.

REFERENCES

1. Kong, L., Fry, M., Al-Samarraie, M., Gilbert, C., and Steinkuller, P.G. (2012). An update on progress and the changing epidemiology of causes of childhood blindness worldwide. J. AAPOS *16*, 501–507.
2. Xu, W., Yin, J., Sun, L., Hu, Z., Dou, G., Zhang, Z., Wang, H., Guo, C., and Wang, Y. (2017). Impact of minocycline on vascularization and visual function in an immature mouse model of ischemic retinopathy. Sci. Rep. *7*, 7535.
3. Xu, W., Hu, Z., Lv, Y., Dou, G., Zhang, Z., Wang, H., and Wang, Y. (2018). Microglial density determines the appearance of pathological neovascular tufts in oxygen-induced retinopathy. Cell Tissue Res. *374*, 25–38.
4. Smith, L.E., Wesolowski, E., McLellan, A., Kostyk, S.K., D'Amato, R., Sullivan, R., and D'Amore, P.A. (1994). Oxygen-induced retinopathy in the mouse. Invest. Ophthalmol. Vis. Sci. *35*, 101–111.
5. Ritter, M.R., Banin, E., Moreno, S.K., Aguilar, E., Dorrell, M.I., and Friedlander, M. (2006). Myeloid progenitors differentiate into microglia and promote vascular repair in a model of ischemic retinopathy. J. Clin. Invest. *116*, 3266–3276.
6. Salter, M.W., and Beggs, S. (2014). Sublime microglia: expanding roles for the guardians of the CNS. Cell *158*, 15–24.
7. Kim, J.H., Kim, J.H., Park, J.A., Lee, S.W., Kim, W.J., Yu, Y.S., and Kim, K.W. (2006). Blood-neural barrier: intercellular communication at glio-vascular interface. J. Biochem. Mol. Biol. *39*, 339–345.
8. Deliyanti, D., Talia, D.M., Zhu, T., Maxwell, M.J., Agrotis, A., Jerome, J.R., Hargreaves, E.M., Gerondakis, S., Hibbs, M.L., Mackay, F., and Wilkinson-Berka, J.L. (2017). Foxp3^{+} Tregs are recruited to the retina to repair pathological angiogenesis. Nat. Commun. *8*, 748.
9. Ebneter, A., Kokona, D., Schneider, N., and Zinkernagel, M.S. (2017). Microglia activation and recruitment of circulating macrophages during ischemic experimental branch retinal vein occlusion. Invest. Ophthalmol. Vis. Sci. *58*, 944–953.
10. Thompson, A.G., Gray, E., Heman-Ackah, S.M., Mäger, I., Talbot, K., Andaloussi, S.E., Wood, M.J., and Turner, M.R. (2016). Extracellular vesicles in neurodegenerative disease - pathogenesis to biomarkers. Nat. Rev. Neurol. *12*, 346–357.
11. Asai, H., Ikezu, S., Tsunoda, S., Medalla, M., Luebke, J., Haydar, T., Wolozin, B., Butovsky, O., Kügler, S., and Ikezu, T. (2015). Depletion of microglia and inhibition of exosome synthesis halt tau propagation. Nat. Neurosci. *18*, 1584–1593.
12. Kalani, A., Tyagi, A., and Tyagi, N. (2014). Exosomes: mediators of neurodegeneration, neuroprotection and therapeutics. Mol. Neurobiol. *49*, 590–600.
13. Moisseiev, E., Anderson, J.D., Oltjen, S., Goswami, M., Zawadzki, R.J., Nolta, J.A., and Park, S.S. (2017). Protective effect of intravitreal administration of exosomes derived from mesenchymal stem cells on retinal ischemia. Curr. Eye Res. *42*, 1358–1367.
14. Fulton, A.B., Reynaud, X., Hansen, R.M., Lemere, C.A., Parker, C., and Williams, T.P. (1999). Rod photoreceptors in infant rats with a history of oxygen exposure. Invest. Ophthalmol. Vis. Sci. *40*, 168–174.
15. Skog, J., Würdinger, T., van Rijn, S., Meijer, D.H., Gainche, L., Sena-Esteves, M., Curry, W.T., Jr., Carter, B.S., Krichevsky, A.M., and Breakefield, X.O. (2008). Glioblastoma microvesicles transport RNA and proteins that promote tumour growth and provide diagnostic biomarkers. Nat. Cell Biol. *10*, 1470–1476.
16. Fulton, A.B., Hansen, R.M., Moskowitz, A., and Akula, J.D. (2009). The neurovascular retina in retinopathy of prematurity. Prog. Retin. Eye Res. *28*, 452–482.
17. Fulton, A.B., Hansen, R.M., Moskowitz, A., and Barnaby, A.M. (2005). Multifocal ERG in subjects with a history of retinopathy of prematurity. Doc. Ophthalmol. *111*, 7–13.
18. Fulton, A.B., Hansen, R.M., and Moskowitz, A. (2008). The cone electroretinogram in retinopathy of prematurity. Invest. Ophthalmol. Vis. Sci. *49*, 814–819.
19. Fulton, A.B., Hansen, R.M., Petersen, R.A., and Vanderveen, D.K. (2001). The rod photoreceptors in retinopathy of prematurity: an electroretinographic study. Arch. Ophthalmol. *119*, 499–505.
20. Vajzovic, L., Rothman, A.L., Tran-Viet, D., Cabrera, M.T., Freedman, S.F., and Toth, C.A. (2015). Delay in retinal photoreceptor development in very preterm compared to term infants. Invest. Ophthalmol. Vis. Sci. *56*, 908–913.
21. Lee, H., Purohit, R., Patel, A., Papageorgiou, E., Sheth, V., Maconachie, G., Pilat, A., McLean, R.J., Proudlock, F.A., and Gottlob, I. (2015). In vivo foveal development using optical coherence tomography. Invest. Ophthalmol. Vis. Sci. *56*, 4537–4545.
22. Akula, J.D., Hansen, R.M., Tzekov, R., Favazza, T.L., Vyhovsky, T.C., Benador, I.Y., Mocko, J.A., McGee, D., Kubota, R., and Fulton, A.B. (2010). Visual cycle modulation in neurovascular retinopathy. Exp. Eye Res. *91*, 153–161.
23. Dembinska, O., Rojas, L.M., Varma, D.R., Chemtob, S., and Lachapelle, P. (2001). Graded contribution of retinal maturation to the development of oxygen-induced retinopathy in rats. Invest. Ophthalmol. Vis. Sci. *42*, 1111–1118.
24. Chiu, W.T., Chang, H.A., Lin, Y.H., Lin, Y.S., Chang, H.T., Lin, H.H., Huang, S.C., Tang, M.J., and Shen, M.R. (2018). Bcl-2 regulates store-operated Ca^{2+} entry to modulate ER stress-induced apoptosis. Cell Death Discov. *4*, 37.
25. Wu, Y., Li, X., Jia, J., Zhang, Y., Li, J., Zhu, Z., Wang, H., Tang, J., and Hu, J. (2018). Transmembrane E3 ligase RNF183 mediates ER stress-induced apoptosis by degrading Bcl-xL. Proc. Natl. Acad. Sci. USA *115*, E2762–E2771.
26. Ansari, S.S., Sharma, A.K., Soni, H., Ali, D.M., Tews, B., König, R., Eibl, H., and Berger, M.R. (2018). Induction of ER and mitochondrial stress by the alkylphosphocholine erufosine in oral squamous cell carcinoma cells. Cell Death Dis. *9*, 296.
27. Kaufman, R.J. (2002). Orchestrating the unfolded protein response in health and disease. J. Clin. Invest. *110*, 1389–1398.
28. Yoshida, H., Matsui, T., Yamamoto, A., Okada, T., and Mori, K. (2001). XBP1 mRNA is induced by ATF6 and spliced by IRE1 in response to ER stress to produce a highly active transcription factor. Cell *107*, 881–891.
29. Son, S.M., Byun, J., Roh, S.E., Kim, S.J., and Mook-Jung, I. (2014). Reduced IRE1α mediates apoptotic cell death by disrupting calcium homeostasis via the InsP3 receptor. Cell Death Dis. *5*, e1188.
30. Zeng, F., Le, Y.G., Fan, J.C., and Xin, L. (2017). Lncrna casc2 inhibited the viability and induced the apoptosis of hepatocellular carcinoma cells through regulating mir-24-3p. J. Cell. Biochem. *119*, 6391–6397.
31. Lu, K., Wang, J., Song, Y., Zhao, S., Liu, H., Tang, D., Pan, B., Zhao, H., and Zhang, Q. (2015). miRNA-24-3p promotes cell proliferation and inhibits apoptosis in human breast cancer by targeting p27Kip1. Oncol. Rep. *34*, 995–1002.
32. Yuan, Y., Kluiver, J., Koerts, J., de Jong, D., Rutgers, B., Abdul Razak, F.R., Terpstra, M., Plaat, B.E., Nolte, I.M., Diepstra, A., et al. (2017). Mir-24-3p is overexpressed in hodgkin lymphoma and protects hodgkin and reed-sternberg cells from apoptosis. Am. J. Pathol. *187*, 1343–1355.
33. Chen, J., and Smith, L.E. (2007). Retinopathy of prematurity. Angiogenesis *10*, 133–140.
34. Heidary, G., Vanderveen, D., and Smith, L.E. (2009). Retinopathy of prematurity: current concepts in molecular pathogenesis. Semin. Ophthalmol. *24*, 77–81.
35. Lahdenranta, J., Pasqualini, R., Schlingemann, R.O., Hagedorn, M., Stallcup, W.B., Bucana, C.D., Sidman, R.L., and Arap, W. (2001). An anti-angiogenic state in mice and humans with retinal photoreceptor cell degeneration. Proc. Natl. Acad. Sci. USA *98*, 10368–10373.
36. Mintz-Hittner, H.A., Kennedy, K.A., and Chuang, A.Z.; BEAT-ROP Cooperative Group (2011). Efficacy of intravitreal bevacizumab for stage 3+ retinopathy of prematurity. N. Engl. J. Med. *364*, 603–615.
37. Stahl, A., Krohne, T.U., Eter, N., Oberacher-Velten, I., Guthoff, R., Meltendorf, S., Ehrt, O., Aisenbrey, S., Roider, J., Gerding, H., et al.; Comparing Alternative Ranibizumab Dosages for Safety and Efficacy in Retinopathy of Prematurity (CARE-ROP) Study Group (2018). Comparing alternative ranibizumab dosages for safety and efficacy in retinopathy of prematurity: A randomized clinical trial. JAMA Pediatr. *172*, 278–286.
38. Chan-Ling, T., Gole, G.A., Quinn, G.E., Adamson, S.J., and Darlow, B.A. (2018). Pathophysiology, screening and treatment of ROP: A multi-disciplinary perspective. Prog. Retin. Eye Res. *62*, 77–119.
39. Khalili, S., Shifrin, Y., Pan, J., Belik, J., and Mireskandari, K. (2018). The effect of a single anti-Vascular Endothelial Growth Factor injection on neonatal growth and organ development: In-vivo study. Exp. Eye Res. *169*, 54–59.
40. Tran, K.D., Cernichiaro-Espinosa, L.A., and Berrocal, A.M. (2018). Management of retinopathy of prematurity–use of anti-vegf therapy. Asia Pac. J. Ophthalmol. (Phila.) *7*, 56–62.

41. György, B., Hung, M.E., Breakefield, X.O., and Leonard, J.N. (2015). Therapeutic applications of extracellular vesicles: clinical promise and open questions. Annu. Rev. Pharmacol. Toxicol. *55*, 439–464.

42. Smith, A.M., Gibbons, H.M., Lill, C., Faull, R.L., and Dragunow, M. (2013). Isolation and culture of adult human microglia within mixed glial cultures for functional experimentation and high-content analysis. Methods Mol. Biol. *1041*, 41–51.

43. Muffat, J., Li, Y., Yuan, B., Mitalipova, M., Omer, A., Corcoran, S., Bakiasi, G., Tsai, L.H., Aubourg, P., Ransohoff, R.M., and Jaenisch, R. (2016). Efficient derivation of microglia-like cells from human pluripotent stem cells. Nat. Med. *22*, 1358–1367.

44. Huang, S., Ge, X., Yu, J., Han, Z., Yin, Z., Li, Y., Chen, F., Wang, H., Zhang, J., and Lei, P. (2018). Increased miR-124-3p in microglial exosomes following traumatic brain injury inhibits neuronal inflammation and contributes to neurite outgrowth *via* their transfer into neurons. FASEB J. *32*, 512–528.

45. al-Ubaidi, M.R., Font, R.L., Quiambao, A.B., Keener, M.J., Liou, G.I., Overbeek, P.A., and Baehr, W. (1992). Bilateral retinal and brain tumors in transgenic mice expressing simian virus 40 large T antigen under control of the human interphotoreceptor retinoid-binding protein promoter. J. Cell Biol. *119*, 1681–1687.

46. Tan, E., Ding, X.Q., Saadi, A., Agarwal, N., Naash, M.I., and Al-Ubaidi, M.R. (2004). Expression of cone-photoreceptor-specific antigens in a cell line derived from retinal tumors in transgenic mice. Invest. Ophthalmol. Vis. Sci. *45*, 764–768.